Proceedings of the ASME 2015 International Design Engineering Technical Conferences & Computers and Information in Engineering Conference
IDETC/CIE 2015
August 2-5, 2015, Boston, USA

DETC2015-47310

DRAFT: INSTANTANEOUS-STIFFNESS PLANE ANALYSIS OF UNDERACTUATED FINGERS

Bruno Belzile
Robotics Laboratory
Department of Mechanical Engineering
Polytechnique Montreal
C.P. 6079, succ. Centre-ville, Montreal, QC H3C 3A7
Email: bruno.belzile@polymtl.ca

Lionel Birglen
Robotics Laboratory
Department of Mechanical Engineering
Polytechnique Montreal
C.P. 6079, succ. Centre-ville, Montreal, QC H3C 3A7
Email: lionel.birglen@polymtl.ca

ABSTRACT

The general stiffness of an underactuated finger as seen from the actuator is a function of its internal compliant elements, such as springs, but also depends on its geometry. In this paper, a complete stiffness analysis of a general underactuated finger is presented. The objective is to shed light on important elements to consider while designing underactuated fingers and how to take advantage of the finger's stiffness during grasping, for instance in order to estimate information such as contact location and force magnitude. This is done using the instantaneous-stiffness plane of the finger introduced in this paper. This plane shows the relationship between the finger's geometry and its instantaneous stiffness and how simple changes in geometrical parameters can have significant effects on the finger's stiffness. This novel tool can be used for a wide range of underactuated finger architectures as will be shown. First, a theoretical framework including numerical simulations is presented. This is then followed by an optimization example of a finger's geometry and a discussion.

1 Introduction

Manipulation and grasping have been important research topics for several decades in robotics, but existing prototypes are still far from being as efficient as the human hand. To have a greater dexterity of robotic hands, the most intuitive solution is to increase the number of actuators. However, the additional actuators also come with greater control complexity, more mass and higher cost. Solutions have been proposed in the literature to deal with these three inconveniences. Underactuated mechanisms for instance are nowadays seen as a promising avenue to this aim. With underactuated robotic finger mechanisms, a.k.a. self-adaptive, mechanical adaptation to the shape of the object seized is used instead of multiple actuators and complex control schemes. The fingers, which are generally either tendon-driven or linkage-driven, combine a transmission mechanism and passive elements such as springs or compliant joints. They are used in a wide field of applications [1–4]. When designing underactuated fingers, one important element to consider lies with the compliant element choice. Indeed, to compensate for the lack of actuators, passive elements are used to constraint the closing and opening motions.

The compliant elements, the transmission mechanism, and its geometry have a significant impact on a finger's behavior during grasping and how efficient it is for grasping (pinch, power) compared to other designs. Indeed, the instantaneous stiffness as seen from the actuator, has a significant impact on the grasp. A high instantaneous stiffness means that the finger is almost completely rigid, no longer adapting itself to the object's shape. On the other hand, a low stiffness is not always a good thing, as the finger could often not resist internal disturbances and therefore, lose the object. Furthermore, the dexterity of an underactuated finger can also be analyzed and optimized in its workspace [5]. The variable stiffness of an underactuated finger can also be used to estimate contact information. Indeed, tactile sensing is a crit-

ical part of the human sensory system. Without it, movement coordination and environment perception could be a challenging task. In robotics, internal and external sensors are used to provide data about the robot itself and its environment. While actual existing sensing systems are very limited compared to a human is, some well chosen and cleverly placed sensors can improve significantly hand's capabilities. Nowadays, external tactile sensors are commonly attached on the phalanges of robotic fingers to provide tactile information. However, other techniques can used to achieve the same objective. Proprioceptive sensors combined with mathematical algorithms, have been shown to be efficient alternatives, mainly for fully actuated fingers [1, 6–9].

In this paper, a new analysis tool, referred to as the instantaneous-stiffness plane, is introduced. This plane illustrates the instantaneous stiffness of sn underactuated finger as a function of its preshaping. An underactuated finger's preshaping is its motion before any contact occurs. On this plane, the instantaneous stiffness for significant locations along the finger is shown. To explain how it works, a kinetostatic modeling of a general underactuated finger is first done. While many kinetostatic analysis of underactuated fingers exist in the literature [10, 12], the one presented here aims at assessing the stiffness as seen from the actuator over the complete workspace of the finger. Then, the instantaneous-stiffness plane is established with different architectures and discussed. Finally, it is used to perform a geometrical optimization.

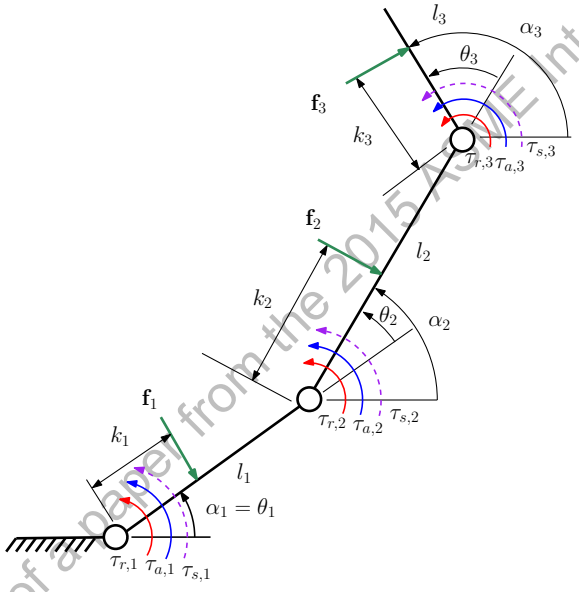

FIGURE 1. UNDERACTUATED FINGER WITH THREE PHALANGES [13].

2 Kinetostatics of Underactuated Fingers

2.1 Basics

Before looking into the kinetostatic analysis of underactuated fingers, the configuration variables of the finger must be defined. First, as shown in Fig. 1, θ_i are the relative angles between successive phalanges. On the other hand, α_i are the absolute angles of each phalanx with respect to the ground. To simplify the equations, the angles θ_i can be put into a vector, i.e.:

$$\boldsymbol{\theta} = \begin{bmatrix} \theta_1 \ \dots \ \theta_n \end{bmatrix}^T. \tag{1}$$

Moreover, θ_a is an angle depending on the actuation mechanism solely (not shown in Fig. 1). The variables k_i are the distance from the origin of a phalanx to the location where a contact force is applied. To simplify the analysis, it is assumed that there is only one normal contact force on each phalanx and that the object grasped is immovable with respect to the base of the finger (the palm in the case of a hand). As with any robotic finger, the forces at the phalanges can be obtained from the Jacobian matrix $\mathbf{J}$ and the equivalent torques at the interphalanx joints:

$$\mathbf{f} = \mathbf{J}^{-\mathbf{T}}\boldsymbol{\tau}, \tag{2}$$

where $\mathbf{J}$ is the Jacobian matrix, $\mathbf{f} = [F_1 F_2 F_3]^T$ the contact force vector, and $\boldsymbol{\tau} = [\tau_1 \tau_2 \tau_3]^T$ the equivalent torque vector at the interphalanx joints [12], as shown in Fig. 1. The Jacobian matrix can be written as:

$$\mathbf{J}^{-T} = \begin{bmatrix} \frac{1}{k_1} & \frac{-\beta_2}{k_1} & \frac{(\beta_2-1)-\psi_3+(\beta_2-1)(\beta_3-1)}{k_1} \\ 0 & \frac{1}{k_2} & \frac{-\beta_3}{k_2} \\ 0 & 0 & \frac{1}{k_3} \end{bmatrix}, \tag{3}$$

with

$$\beta_i = 1 + \frac{l_{i-1}\cos\theta_i}{k_i}, \psi_3 = \frac{l_1\cos(\theta_2+\theta_3)}{k_3}. \tag{4}$$

where l_i is the length of the i^{th} phalanx. For a two-phalanx finger, the Jacobian matrix is the (2×2) upper left part of the three-phalanx Jacobian matrix. It should be pointed out that $\beta_2 k_2$ is also equal to the lever-arm distance of the contact force with respect to the origin of the finger. Equivalently, for a contact force on the third phalanx, one interesting property of these parameters is that $k_3(\beta_3+\psi_3)$ is equal to the lever-arm distance

with respect to the base joint of the finger. These torques in $\boldsymbol{\tau}$ can be produced by active elements (e.g. actuators) and/or passive elements (e.g. springs). If these elements are not located at the joints, a transformation matrix $\mathbf{P}$ can be used to obtain $\boldsymbol{\tau}$ from the torques applied at the actuated joints $\boldsymbol{\tau}_a$:

$$\boldsymbol{\tau} = \mathbf{P}^T \boldsymbol{\tau}_a + \mathbf{x} T_a, \tag{5}$$

where T_a is the actuation torque and $\mathbf{x}$ is a vector containing every transmission factors, as defined in [12]. For example, this last vector is generally a function of the pulleys' radii in tendon-driven mechanism. If $\boldsymbol{\tau}$ is defined as a function of the equivalent torques generated at the interphalanx joints, one has:

$$\boldsymbol{\tau} = \mathbf{T}^{*T} \left[T_a \; T_1 \; T_2 \; \dots \; T_n \right]^T, \tag{6}$$

where T_i is the torque generated at the i$^{\text{th}}$ interphalanx joint. Also, one has:

$$\mathbf{T}^{*T} = \left[\mathbf{x} \; \mathbf{I} \right], \tag{7}$$

where the matrix $\mathbf{I}$ is the $n \times n$ identity matrix and the vector $\mathbf{x}$ is defined by:

$$\mathbf{x} = \left[\frac{1}{X_1} \; -\frac{X_2}{X_1} \; \dots \; -\frac{X_n}{X_1} \right]^T. \tag{8}$$

The parameters X_i depend on the transmission mechanism. The dynamic effect in the system are not considered because of the low kinetic energy generally involved in underactuated grasping [11]. The vector $\boldsymbol{\tau}$ can be written with the stiffness coefficients of the compliant elements and the transmission coefficients of the linkage mechanism as:

$$\tau = \mathbf{P}^T \mathbf{K} \Delta\theta_a + \mathbf{x} T_a, \tag{9}$$

where $\Delta\boldsymbol{\theta}_a$ is the variation of the relative angles at the joints where compliant elements are located and with $\mathbf{K}$ defined as:

$$\mathbf{K} = \begin{bmatrix} K_1 & 0 & 0 \\ 0 & K_2 & 0 \\ 0 & 0 & K_3 \end{bmatrix}. \tag{10}$$

The parameters K_i are the stiffness coefficients of the passive compliant joints not to be confused with the contact locations k_i.

2.2 Geometric Closure

Along with the contact forces, another important element for the analysis of underactuated fingers is the geometric closure. Theoretically, from the vector $\mathbf{x}$, it is possible to compute the geometric-loop equation by integrating its product with $\Delta\boldsymbol{\theta}$ with respect to time. This equation links all the independent angles of the mechanism. Its general formulation is:

$$\Delta\theta_a = \int \mathbf{x}^T (\boldsymbol{\theta} - \boldsymbol{\theta}_0) dt. \tag{11}$$

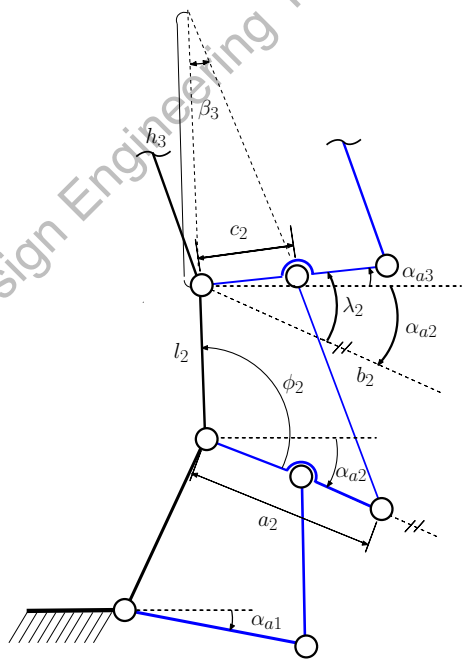

FIGURE 2. GEOMETRY OF A TYPICAL LINKAGE-DRIVEN FINGER.

In the case of a linkage-driven finger (e.g. Fig. 2), the equation is however quite complex and challenging to solve because $\mathbf{x}$ depends on the geometrical configuration. However, by using the Weierstrass substitution, it is possible to obtain an explicit input-output equation giving α_{k+1} as a function of $\alpha_{k,a}$ for each four-bar linkage defining the transmission mechanism. This equation is very similar to the Freudenstein equation presented in [14]. Thus, for each linkage, one has:

$$\zeta_1 - \zeta_2 \cos\phi_i - \zeta_3 \cos\lambda_i + \cos(\phi_i - \lambda_i) = 0, \tag{12}$$

where

$$\zeta_1 = \frac{l_i^2 + c_i^2 + a_i^2 - b_i^2}{2 l_i c_i},\ \zeta_2 = \frac{a_i}{c_i},\ \zeta_3 = \frac{a_i}{l_i}. \tag{13}$$

By manipulating the variables, one can rewrite Eq. (12) in the following form:

$$A_i \cos\phi_i + B_i \sin\phi_i + C_i = 0, \tag{14}$$

where

$$A_i = \cos\lambda_i - \zeta_2,\ B_i = \sin\lambda_i,\ C_i = \zeta_1 - \zeta_3 \cos\lambda_i. \tag{15}$$

Setting $T_i = \tan(\phi_i/2)$, the following quadratic equation is then obtained:

$$D_i(\lambda_i)T^2 + E_i(\lambda_i)T + F_i(\lambda_i) = 0, \tag{16}$$

where

$$D_i = C_i - A_i,\ E_i = 2B_i,\ F_i = A_i + C_i. \tag{17}$$

By computing the inverse tangent of the roots of Eq. (16), one finally obtains an equation for ϕ_i as a function of λ_i. Knowing that $\alpha_i = \phi_i + \alpha_{ai}$, a general function $\alpha_a = g(\alpha_1, \alpha_{a2}, ..., \alpha_{an})$ is achieved.

2.3 Preliminary Analysis

Prior to completing a full stiffness analysis of linkage-driven fingers, a first step can be done by making a preliminary analysis without expressing every equations. The instantaneous stiffness K_c of a underactuated finger as seen from the actuator, can be very useful when designing an underactuated finger. Note that the global stiffness is created by the springs (or equivalent compliant elements) at the joints, and not the links of the finger themselves. Many examples of this can be found in the literature [2, 16]. First, the instantaneous stiffness of the finger is defined as:

$$K_c = \frac{dT_a}{d\theta_a}, \tag{18}$$

namely the derivative of T_a, the required actuation torque to achieved static equilibrium, with respect to θ_a, the actuator angular position. To expand this equation, derivatives are needed. However, because the X_i terms are not constant with respect to θ_a, an alternative to expressing the derivatives of these variables (which can be challenging) is to compute the finger configuration for an actuation torque equal to $(T_{a,i} + \Delta T_a)$. The original equations before differentiating with respect to T_a are used for this. It consists of the null contact force equation, i.e Eq. (2) for the lines where $F_i = 0$, the geometric closure equation (Eqs. (11, 16) or the equation corresponding to the chosen mechanism) and the geometric equation defining the absolute coordinates of the contact location, which is a function of the finger's configuration (described by $\boldsymbol{\theta}$). The variables are the angles θ_i, which are not known in this case because of the torque variation, instead of the $d\theta_i/dT_a$. The equations are not linear for these parameters, it is therefore not possible to obtain a simple explicit function for K_c. Instead, the set of equations must be solved numerically to obtain every parameters of the following equation, which is an approximation of K_c:

$$K_c = \frac{dT_a}{dx_a} \approx \frac{\Delta T_a}{\Delta x_a}. \tag{19}$$

TABLE 1. GEOMETRIC PARAMETERS OF TYPICAL UNDERACTUATED FINGERS.

2-DOF linkage A		2-DOF linkage B		3-DOF tendon	
L_1	1	L_1	1	L_1	1
L_2	1	L_2	0.75	L_2	0.75
a_1	1	a_1	0.50	L_3	0.50
b_1	1	b_1	1	r_1	0.10
c_1	1/3	c_1	1/3	r_2	0.08
ϕ_2	$\pi/2$	ϕ_2	$\pi/2$	r_3	0.06
$\theta_{i,0}$	$\pi/4$	$\theta_{i,0}$	$\pi/4$	r_4	0.04
				$\theta_{i,0}$	$\pi/6$

This is only valid for a small ΔT_a. The solid curve (SA) in Fig. 3 is obtained using this method. The second curve is obtained with a dynamic simulation package (DSP) to compare the results. The divergence near e_2, the equilibrium position [12], is caused by the very high stiffness of the finger making it impossible to have an accurate value of K_c with the DSP. The latter

considers a contact stiffness that is not taken into account in our theoretical model. The equilibrium position, resulting in an infinite stiffness, is defined by:

$$e_2 = \frac{-l_1 \cos\theta_2 X_2}{X_2 + 1}. \tag{20}$$

The geometric parameters of this example (linkage-driven finger A) are shown in Table 1. Throughout the paper, for numerical simulations, the stiffnesses K_i used are always equal to 1. The divergence near e_2 can actually also be observed with an actual physical finger. In this case, it is caused by internal deformations of the finger.

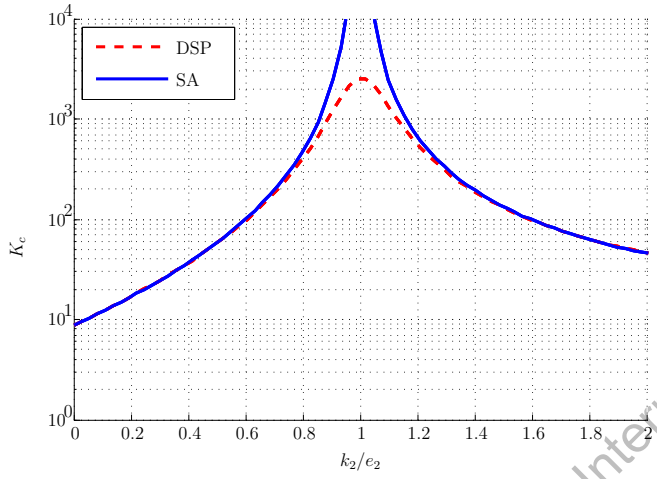

FIGURE 3. INSTANTANEOUS STIFFNESS ESTIMATION.

2.4 Reduced Equation System

The next step in the analysis is to eliminate the unknown contact forces during grasping from the equations. Indeed, every elements of $\mathbf{f}$ not equal to zero must be eliminated from the equation system, because the contact forces are not known. Furthermore, the undefined k_i must be eliminated to pursue the analysis. Thus, if $\mathbf{J}^{-T}$ is defined as $\begin{bmatrix}\mathbf{j}_1 \ \mathbf{j}_2 \ \dots \ \mathbf{j}_k \ \dots \ \mathbf{j}_n\end{bmatrix}^T$, then $\mathbf{J}_k^*$ is defined for a contact on the k^{th} phalanx and can be expressed as $\begin{bmatrix}\mathbf{j}_1 \ \mathbf{j}_2 \ \dots \ \mathbf{j}_{k-1} \ \mathbf{j}_{k+1} \ \dots \ \mathbf{j}_n\end{bmatrix}^T$. From the original Jacobian matrix, the following reduced matrices (for a single initial contact on the proximal, intermediate, or distal phalanx of a finger) can be obtained:

$$\mathbf{J}_1^* = \begin{bmatrix}0 & 1 & 0\\ 0 & 0 & 1\end{bmatrix}, \tag{21}$$

$$\mathbf{J}_2^* = \begin{bmatrix}1 & -\beta_2 & 0\\ 0 & 0 & 1\end{bmatrix}, \tag{22}$$

$$\mathbf{J}_3^* = \begin{bmatrix}1 & 0 & -\beta_3 - \psi_3\\ 0 & 1 & -\beta_3\end{bmatrix}. \tag{23}$$

As with the original Jacobian matrix $\mathbf{J}$, the equivalent reduced matrices for a two-phalanx finger are the first two elements of the first lines of the previous matrices.

3 Instantaneous-Stiffness Plane

As previously stated, the objective of this paper is to obtain the instantaneous-stiffness plane of underactuated fingers. To achieve this, one needs a general expression of K_c. The first step is to differentiate Eq. (2) with respect to the actuation torque T_a. However, before doing so, one can simplify Eq. (2) by using $\mathbf{J}_i^*$ as defined above, i.e. $\mathbf{J}_i^*\boldsymbol{\tau} = \mathbf{0}$, in the case of a contact on the i^{th}. By differentiating, the equation becomes:

$$\frac{d\mathbf{J}_i^*}{dT_a}\boldsymbol{\tau} + \mathbf{J}_i^*\frac{d\boldsymbol{\tau}}{dT_a} = \mathbf{0}. \tag{24}$$

Knowing that, when no contact force is generated by the finger, $\boldsymbol{\tau}$ is null, one can simplify the previous equation at the instant of contact, just before the contact force starts increasing. By expanding the derivative, one obtains:

$$\mathbf{J}_i^*\left(\frac{d\mathbf{x}}{dT_a}T_a - \frac{d\mathbf{P}^T}{dT_a}\mathbf{K}\Delta\boldsymbol{\theta}_a - \mathbf{P}^T\mathbf{K}\frac{d\boldsymbol{\theta}_a}{dT_a} + \mathbf{x}\right) = \mathbf{0}. \tag{25}$$

The first term in the parenthesis of this equation can be rewritten as:

$$\frac{d\mathbf{x}}{dT_a}T_a = \frac{\partial\mathbf{x}}{\partial\boldsymbol{\theta}}\frac{d\boldsymbol{\theta}}{dT_a}T_a = \mathbf{G}\frac{d\boldsymbol{\theta}}{dT_a}. \tag{26}$$

where $\mathbf{G}$ is the product of actuation torque and the mathematical Jacobian of $\mathbf{x}$ with respect to $\boldsymbol{\theta}$, i.e.:

$$\mathbf{G} = \begin{bmatrix} \frac{\partial x_1}{\partial \theta_1} & \frac{\partial x_1}{\partial \theta_2} & \cdots & \frac{\partial x_1}{\partial \theta_n} \\ \frac{\partial x_2}{\partial \theta_1} & \frac{\partial x_2}{\partial \theta_2} & \cdots & \frac{\partial x_2}{\partial \theta_n} \\ \vdots & \vdots & \ddots & \vdots \\ \frac{\partial x_n}{\partial \theta_1} & \frac{\partial x_n}{\partial \theta_2} & \cdots & \frac{\partial x_n}{\partial \theta_n} \end{bmatrix} T_a. \tag{27}$$

The second term can also be manipulated to express the term $d\boldsymbol{\theta}/dT_a$. First, it can be rewritten as:

$$\frac{d\mathbf{P}^T}{dT_a}\mathbf{K}\Delta\boldsymbol{\theta}_a = \sum_{j=1}^{n}\left(\mathbf{P}_i'^T\frac{\theta_j}{T_a}\right)\mathbf{K}\Delta\boldsymbol{\theta}_a, \tag{28}$$

where the matrices $\mathbf{P}_i'^T$ are obtained by differentiating $\mathbf{P}^T$ with respect to the phalanx relative angle θ_i. With some manipulations, this following final expression is obtained:

$$\begin{aligned} \frac{d\mathbf{P}^T}{dT_a}\mathbf{K}\Delta\boldsymbol{\theta}_a = \mathbf{W}\frac{d\boldsymbol{\theta}}{dT_a} = \\ \left[\mathbf{P}_1'^T\mathbf{K}\Delta\boldsymbol{\theta}_a\ \mathbf{P}_2'^T\mathbf{K}\Delta\boldsymbol{\theta}_a\ \ldots\ \mathbf{P}_n'^T\mathbf{K}\Delta\boldsymbol{\theta}_a\right]\frac{d\boldsymbol{\theta}}{dT_a}. \end{aligned} \tag{29}$$

Finally, the third term in Eq. (25) can be written as:

$$\mathbf{P}^T\mathbf{K}\frac{d\boldsymbol{\theta}_a}{dT_a} = \mathbf{P}^T\mathbf{K}\mathbf{P}\frac{d\boldsymbol{\theta}}{dT_a}. \tag{30}$$

Furthermore, one also has:

$$\frac{d\theta_a}{dT_a} = \mathbf{x}^T\frac{d\boldsymbol{\theta}}{dT_a} = \frac{1}{K_c}. \tag{31}$$

To have a fully determined system of equations, one has to add the contact closure equation, which depends on the phalanx where the contact happens. This equation is obtained by differentiating the geometric closure equation from the base of the finger to the point of contact on the k^{th} phalanx. Its general form is the following:

$$\boldsymbol{\Gamma}_i^T\frac{d\boldsymbol{\theta}}{dT_a} = 0, \tag{32}$$

where $\boldsymbol{\Gamma}_i$ contains the coefficients which depend on the contact phalanx and specific location. The possible values of $\boldsymbol{\Gamma}_i$ are:

$$\boldsymbol{\Gamma}_1 = \begin{bmatrix}1\ 0\ 0\end{bmatrix}^T, \tag{33}$$

$$\boldsymbol{\Gamma}_2 = \begin{bmatrix}\beta_2\ 1\ 0\end{bmatrix}^T, \tag{34}$$

$$\boldsymbol{\Gamma}_3 = \begin{bmatrix}\beta_3+\psi_3\ \beta_3\ 1\end{bmatrix}^T, \tag{35}$$

respectively for the proximal, intermediate and distal phalanges. If a two-phalanx finger is considered, only the first two elements are used for $\boldsymbol{\Gamma}_1$ and $\boldsymbol{\Gamma}_2$. The final step to obtain an instantaneous-stiffness equation is to combine Eqs. (25), (31) and (32):

$$K_c^{-1} = \mathbf{x}^T\begin{bmatrix}\mathbf{J}_i^*(\mathbf{P}^T\mathbf{K}\mathbf{P}-\mathbf{G}-\mathbf{W}) \\ \boldsymbol{\Gamma}_i^T\end{bmatrix}^{-1}\begin{bmatrix}\mathbf{J}_i^* \\ \mathbf{0}^T\end{bmatrix}\mathbf{x}. \tag{36}$$

If the passive compliant elements are located directly between the phalanges, $\mathbf{P}$ is equal to the identity matrix and $\mathbf{W}$ to the null matrix. While mechanical limits can be added to this modeling, they are not considered here to simplify the equations. Furthermore, the finger's motion being distributed to all the joints, these limits should not be reached inside the normal workspace.

Using Eq. (36), it is possible to compute the instantaneous-stiffness plane for the complete workspace of the finger. For a two-phalanx finger, an example is given in Fig. 4 (2-DOF linkage-driven finger B, cf. Table 1). The curves on the figure represent the instantaneous stiffness for contacts on particularly significant locations, such as the phalanx extreme points and the locations where K_c reaches a maximum or a minimum. The acronyms IPS and DPS in this figure signify respectively "intermediate phalanx solution" and "distal phalanx solution." Thus, an area of this figure where "2 IPS" is written means that there are two possible solutions on the intermediate phalanx. Also, every contacts on the proximal phalanx being equivalent from the actuation point of view, the curve CPP means that every solutions on the proximal phalanx exist along that curve. Thus, it is impossible to estimate the location of a contact force on the proximal phalanx with only measurements made on the actuator. This does not apply for the intermediate and distal phalanges.

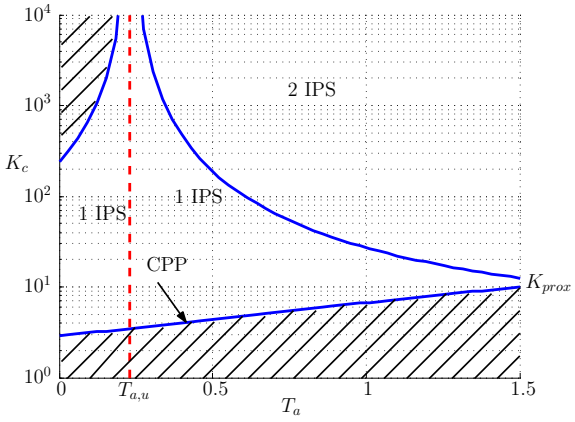

FIGURE 4. INSTANTANEOUS-STIFFNESS PLANE FOR THE TWO-PHALANX FINGER B.

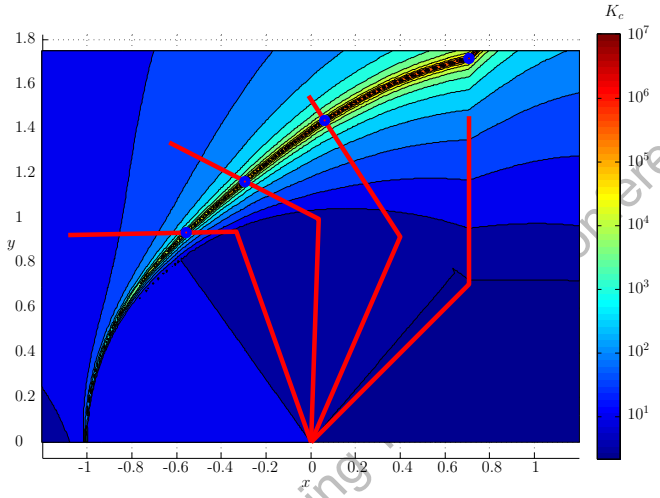

FIGURE 5. INSTANTANEOUS-STIFFNESS MAP OF THE WORKSPACE OF THE FINGER B.

This example illustrated in Fig. 4 is actually of a deficient geometry, because after $T_{a,u}$ ($T_{a,u} = 0.23$ for these parameters), no matter the value of T_a, there is a location ($k_2 = e_2$) on the distal phalanx where a contact results into a infinite stiffness, thus a complete static equilibrium of the finger. There is therefore no adaptation to the shape of the object for grasping. Thus, over the "CCP" curve, every possible K_c exist. From $k_2 = 0$ to $k_2 = e_2$, K_c increases toward infinity. Then, for $k_2 > e_2$, K_c decreases until it reaches the curve above "CCP" for contacts at the end of the second phalanx. For $k_2 > e_2$, θ_2 decreases with the input torque, resulting in a possible ejection of the object. The instantaneous stiffness of the "CCP" curve, K_{prox}, can be computed with Eq. (37). In the case of an architecture with constant transmission coefficients X_i, the value of K_{prox} is constant. The value of $T_{a,u} = 0.23$ was actually verified experimentally on a prototype with an error of approximately 9%, which suggests the equations are valid. The formula to compute the instantaneous stiffness for contacts on the proximal phalanx (i.e. the CPP curve) is:

$$K_{prox,2} = -(X_1^2(g_{22} - K_2))/X_2^2, \tag{37}$$

where g_{ij} are elements of the matrix $\mathbf{G}$. Thus, if the transmission coefficients are constant, $K_{c,prox}$ is also a constant. With the same equations, it is also possible to map the instantaneous stiffness on the complete workspace of the finger. For the two-phalanx linkage-driven finger used in this section, the instantaneous-stiffness map is shown in Fig. 5. The highest stiffness zone in this figure is correspond to a distal contact at e_2 for every possible poses of the finger before contact.

Another example is given in Fig. 6, in this case for a three-phalanx tendon-driven finger (such as the *Soft-gripper* [16]). The geometrical parameters used are given in Table 1.

As it can be seen in Fig. 6, four zones can be defined on the plot. In Zone 1, no solution exists. In Zone 2, the only contact possible are along the distal phalanx, with a low instantaneous-stiffness. In Zone 3, contacts are possible on every phalanges. Finally, in Zone 4, only contacts on the distal phalanx are possible, here with a high instantaneous stiffness. The limits between the zones, namely K_{dist}, K_{prox} and K_{inf}, can be computed using simple equations. First, K_{dist} can be found by differentiating Eq. (36) with respect to k_i for a contact occurring on the intermediate phalanx. It can be shown that β_2 is equal to $1/X_2$ when K_c reaches its maximum value. Thus, from this result, it is possible to compute the maximum value K_c can reach for a contact on the second phalanx. In the case of a mechanism where $\mathbf{G}$ is equal to the null matrix (which is the case of many common tendon-driven fingers), $K_{dist,3}$ can be computed with the following equation:

$$K_{dist,3} = K_3 \left(X_1/X_3\right)^2. \tag{38}$$

To compute $K_{prox,3}$, it can be simply done using Eq. (36) and the parameters for a contact on the first phalanx (again with $\mathbf{G} = \mathbf{0}$), i.e.:

$$K_{prox,3} = \frac{X_1^2}{X_2^2/K_2 + X_3^2/K_3 + 1}. \tag{39}$$

One of the most important element to look in Fig. 6 is the separation at $T_{a,u}$. Before this line, for each contact location k_i, there is an unique corresponding K_c and vice versa. However, after this line, there can be a particular K_c could be valid for

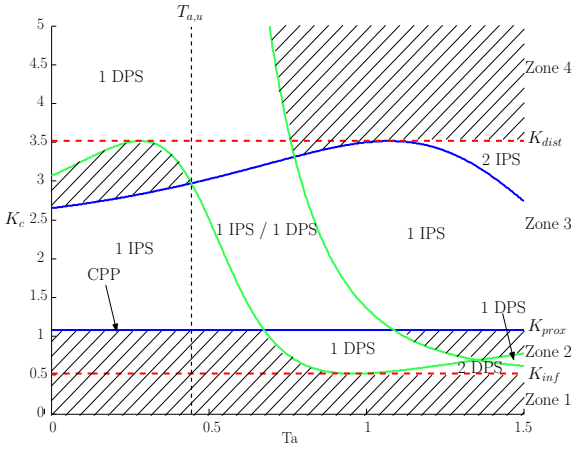

FIGURE 6. INSTANTANEOUS-STIFFNESS PLANE FOR THE SOFT-GRIPPER FINGER C.

multiple k_i. Thus, at least one additional sensor is required to establish the valid contact location.

To compute $T_{a,u}$, one has to obtain T_a from the following equation:

$$K_c|_{i=2}^{k_i=l_i} = K_c|_{i=3}^{k_i=0}. \tag{40}$$

Finally, $T_{a,f}$ is defined as the input torque reached when α_3, the distal phalanx absolute angle, is equal to π, which is chosen as the arbitrary end of the finger's preshaping workspace for the purpose of the optimization.

The instantaneous-stiffness map of this three-phalanx tendon-driven finger is shown in Fig. 7. Contrary to the linkage-driven finger, it can be seen that the complete area swept by the proximal phalanx has a constant stiffness, because the vector $\mathbf{x}$ is also constant. The second posture illustrated from the right, computed right after $T_a = T_{a,u}$, shows that, from this point, there are locations on the intermediate and distal phalanges with the same stiffness. Indeed, the stiffness decreases after this point, changing from dark red to blue in this figure for the distal phalanx.

3.1 Null Stiffness at the Base

Based on the simulation results and the experimental data obtained previously, it has been noted that by removing the compliant element between the palm and the proximal phalanx (or having a notably lower stiffness than the other elements), the instantaneous-stiffness plane was significantly simpler. Indeed, during the preshaping motion of the finger before a contact is made, the configuration of the finger (i.e., the vector $\boldsymbol{\theta}$) remains the same, apart of the angle θ_1. Because the instantaneous stiffness is never a function of θ_1 for the architectures presented in

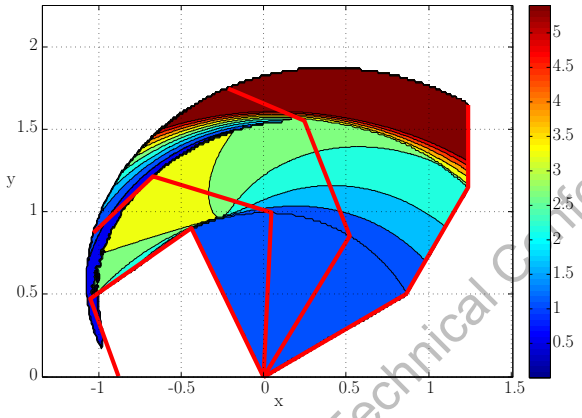

FIGURE 7. INSTANTANEOUS-STIFFNESS MAP OF THE WORKSPACE OF FINGER C.

this paper (where $X_1 = 1$), no matter when the contact occurs, the instantaneous stiffness only depends on the contact location k_i, and it is no longer a function of θ_a. Mathematically, the equations are also simplified since $T_{a,c}$ must be equal to zero in quasi-static conditions. Thus, $\mathbf{G}$ has to be equal to $\mathbf{0}$.

While being an interesting special case, it is also common among many existing underactuated fingers since it keeps the finger in full extension before contact. The instantaneous-stiffness map of the previous tendon-driven finger, with the same parameters except $K_1 = 0$, is shown in Fig. 8 for illustration.

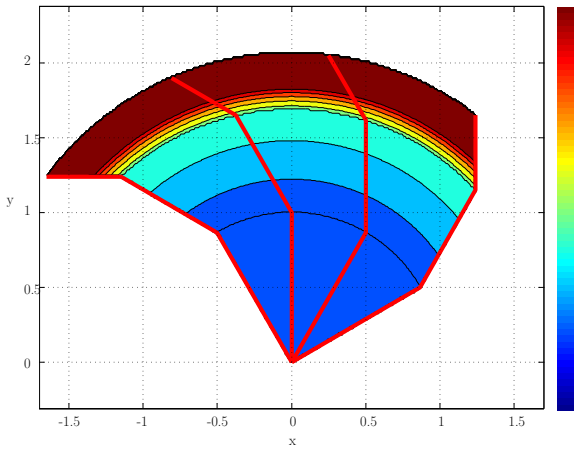

FIGURE 8. INSTANTANEOUS-STIFFNESS MAP WITH $K_1 = 0$.

3.2 Multiple contacts

In the case of multiple simultaneous contacts, the previous equations can be adapted. Having other elements of $\mathbf{f}$ not equal to zero eliminates an equivalent number of equations. However,

this can be compensated by adding the same number of contact closure equations $\boldsymbol{\Gamma}_i$. Therefore, a solvable system of equations can be obtained. The matrix $\mathbf{B}$ stays the same and the matrix $\mathbf{A}$ becomes:

$$\mathbf{A} = \begin{bmatrix} \mathbf{J}_{ij}^{*}(\mathbf{K}-\mathbf{G}) \\ \boldsymbol{\Gamma}_i^T \\ \boldsymbol{\Gamma}_j^T \end{bmatrix}, \tag{41}$$

when a simultaneous contact occurs on the i^{th} and j^{th} phalanges. The possible values of $\mathbf{J}_{ij}^{*}$, where i and j are the indexes of the phalanges in contact with an object, are:

$$\mathbf{J}_{12}^{*} = \begin{bmatrix} 0 & 0 & 1 \end{bmatrix}, \tag{42}$$

$$\mathbf{J}_{13}^{*} = \begin{bmatrix} 0 & 1 & -\beta_3 \end{bmatrix}, \tag{43}$$

$$\mathbf{J}_{23}^{*} = \begin{bmatrix} 1 & -\beta_2 & (\beta_2-1)-\psi_3+(\beta_2-1)(\beta_3-1) \end{bmatrix}. \tag{44}$$

As shown in Fig. 9, a single value of K_c is equivalent to a complete range of contact combinations. However, the instantaneous stiffness induced by any contact combination is generally significantly higher than it can be for a single contact.

The instantaneous-stiffness plane including the two-simultaneous contact scenario is shown in Fig. 10. The acronym 1CS and 2CS stand for respectively *one-contact solution* and *two-contact solution*. It can be seen that the instantaneous stiffness for a double simultaneous contact is generally higher than for a single contact, with a zone where both are possible.

3.3 Geometrical Optimization

There are many ways to improve and optimize the geometry of an underactuated finger, depending of the objective aimed. While the length of the phalanges are usually a design choice based on the application, the parameters of the transmission mechanism can be modified more easily. Even though the theoretical model does not take into account some phenomenon such as friction and dynamic effects and that some discrepancies are to be expected when a practical prototype is used, it should be accurate enough to make it possible to optimize the geometrical parameters to improve performance.

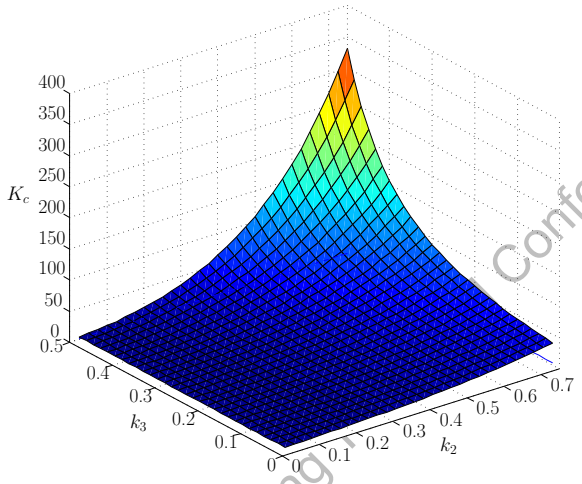

FIGURE 9. MULTIPLE CONTACT INSTANTANEOUS STIFFNESS.

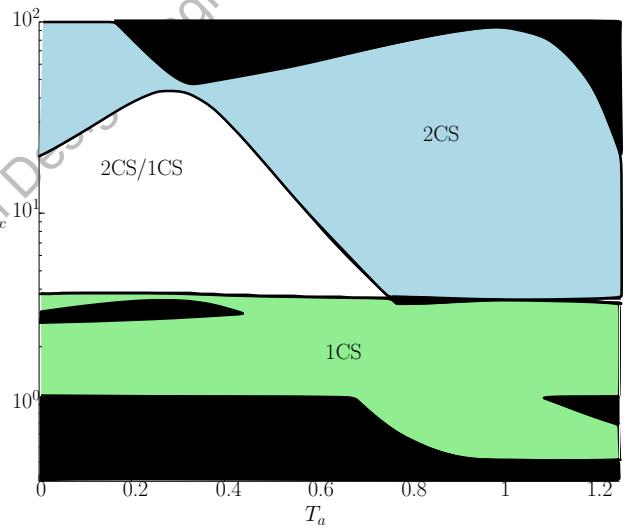

FIGURE 10. INSTANTANEOUS-STIFFNESS PLANE INCLUDING SIMULTANEOUS CONTACTS.

For example, the geometry of an underactuated finger can be optimized to avoid an infinite instantaneous stiffness within the finger's workspace. Indeed, for a two-phalanx finger, if the contact location is equal to e_2, there is no longer any adaptation to the object's shape. Thus, the force applied only push the object rather grasping it. The following performance index can be used:

$$P = \frac{T_{a,u}}{T_{a,f}} \frac{e_{2,f}}{l_2}, \tag{45}$$

where $T_{a,u}$ is the actuation torque when $e_2 = l_2$ and $e_{2,f}$ is the infinite-stiffness location when $T_a = T_{a,f}$. Arbitrary, one can

define the final value of the actuation torque $T_{a,f}$ as the actuation torque needed to close the finger, for example to have $\alpha_2 = 3\pi/2$ for a two-phalanx finger. By optimizing the parameters a and b of the linkage-driven finger B using genetic algorithms, one obtains respectively 0.485 and 0.850. This design is significantly improved, with $P = 0.3038$, which is nearly five times the original value.

4 Conclusion

In this paper, a theoretical model of an underactuated finger was presented to introduce the instantaneous-stiffness plane. This tool is useful to understand the behavior of the finger during grasping. It can be used to choose the architecture and optimize the geometrical parameters of these fingers. It is also useful to assess the possibility of proprioceptive tactile sensing. Throughout the paper, simulations were used to validate the equations. Future work will be focused on designing a complete robotic hand using the instantaneous-stiffness plane.

Acknowledgment

This work was supported by the National Science and Engineering Research Council (NSERC) as well as the Fonds de recherche du Québec - Nature et technologies and the Canadian Foundation for Innovation.

REFERENCES

[1] B. Belzile and L. Birglen, "A compliant self-adaptive gripper with proprioceptive haptic feedback," *Autonomous Robots*, DOI: 10.1007/s10514-013-9360-1, pp. 1–13, 2013.

[2] M. Ciocarlie, F. M. Hicks, R. Holmberg, J. Hawke, M. Schlicht, J. Gee, S. Stanford, and R. Bahadur, "The velo gripper: A versatile single-actuator design for enveloping, parallel and fingertip grasps," *International Journal of Robotics Research*, doi: 10.1177/0278364913519148, pp. 1–15, 2014.

[3] J. Borras and A.M. Dollar, "Analyzing dexterous hands using a parallel robots framework," *Autonomous Robots*, vol. 36, no. 1-2, pp. 169-180, 2014.

[4] D. Aukes, B. Heyneman, J. Ulmen, H. Stuart, M. R. Cutkosky, S. Kim, P. Garcia, and A. Edsinger, "Design and testing of a selectively compliant underactuated hand," *International Journal of Robotics Research*, doi: 10.1177/0278364913518997, pp. 1–15, 2014.

[5] R.R. Ma and A.M. Dollar, "Linkage-Based Analysis and Optimization of an Underactuated Planar Manipulator for In-Hand Manipulation," *ASME Journal of Mechanisms and Robotics*, vol. 6, no. 1, pp. 011002-1-9, 2014.

[6] M. Kaneko and K. Tanie, "Contact point detection for grasping an unknown object usign self-posture changeability," *IEEE Transactions on Robotics and Automation*, vol. 10, no. 3, pp. 355–367, 1994.

[7] M. Huber and R. A. Grupen, "2-d contact detection and localization using proprioceptive information," *IEEE Transactions on Robotics and Automation*, vol. 10, pp. 23–33, 1994.

[8] S. Haidacher and G. Hirzinger, "Contact point identification in multi-fingered grasps exploiting kinematic constraints," in *Proc. IEEE International Conference on Robotics and Automation (ICRA'02)*, vol. 2, Washington, D.C., May 2002, pp. 1597–1603.

[9] G.S. Koonjul, G.J. Zeglin, and N.S. Pollard, "Measuring contact points from displacements with a compliant, articulated robot hand," in *Proc. IEEE International Conference on Robotics and Automation (ICRA'11)*, Shanghai, China, May 2011, pp. 489–495.

[10] A. Battezzato, "Towards an underactuated finger exoskeleton: An optimization process of a two-phalange device based on kinetostatic analysis," *Mechanism and Machine theory*, vol. 78, pp. 116–130, 2014.

[11] R. Ozawa, H. Kobayashi, and K. Hashirii, "Analysis, Classification, and Design of Tendon-Driven Mechanisms," *IEEE Transactions on Robotics and Automation*, vol. 30, no. 2, pp. 396–410, 2014.

[12] L. Birglen, T. Laliberté, and C. Gosselin, *Underactuated Robotic Hands*, B. Siciliano, O. Khatib, and F. Groen, Eds. Springer Tracts in Advanced Robotics, 2008.

[13] B. Belzile and L. Birglen, "Stiffness Analysis of Double Tendon Underactuated Finger," in *Proc. IEEE International Conference on Robotics and Automation (ICRA'14)*, Hong Kong, Jun. 2014.

[14] S. Bai and J. Angeles, "A unified input-output analysis of four-bar linkages," *Mechanism and Machine Theory*, vol. 43, no. 2, pp. 240–251, February 2008.

[15] T. Bergquist, C. Schenck, U. Ohiri, J. Sinapov, S. Griffith, and A. Stoytchev, "Interactive object recognition using proprioceptive feedback," in *Proc. IROS Workshop: Semantic Perception for Robot Manipulation*, St. Louis, MO, Oct. 2009.

[16] S. Hirose and Y. Umetani, "Development of soft gripper for the versatile robot hand," *Mechanism and Machine Theory*, vol. 13(3), pp. 351–359, 1978.